Plasmonic Nickel Nanoantennas

Jianing Chen[1,2], Pablo Albella[1,2], Zhaleh Pirzadeh[3], Pablo Alonso-González[1], Florian Huth[1], Stefano Bonetti[5], Valentina Bonanni[3,5], Johan Åkerman,[4,5] Josep Nogués[6,7], Paolo Vavassori[1,8], Alexandre Dmitriev[3], Javier Aizpurua[2], Rainer Hillenbrand[1,8]

1 CIC nanoGUNE Consolider, 20018 Donostia-San Sebstián, Spain

2 Centro de Fisica de Materiales (CSIC-UPV/EHU) and Donostia International Physics Center (DIPC), 20018 Donostia-San Sebastián, Spain

3 Department of Applied Physics, Chalmers University of Technology, 41296 Gothenburg, Sweden

4 Department of Physics, University of Gothenburg, 412 96 Gothenburg, Sweden

5 Materials Physics, Royal Institute of Technology (KTH), Electrum 229, 164 40 Kista, Sweden

6 CIN2(ICN-CSIC) and Universitat Autónoma de Barcelona, Catalan Institute of Nanotechnology (ICN), Campus UAB, 08193 Bellaterra (Barcelona), Spain

7 Institució Catalana de Recerca i Estudis Avancats(ICREA), Barcelona, Spain

8 IKERBASQUE, Basque Foundation for Science, 48011 Bilbao, Spain

R. Hillenbrand Corresponding-Author r.hillenbrand@nanogune.eu

We study the fundamental optical properties of pure nickel nanostructures by far-field extinction spectroscopy and optical near-field microscopy, providing direct experimental evidence of the existence of particle plasmon resonances predicted by theory. Experimental and calculated near-field maps allow for unambiguous identification of dipolar plasmon modes. By comparing calculated near-field and far-field spectra, we find dramatic shifts between the near-field and far-field plasmon resonance, which are much stronger than in gold nanoantennas. Based on a simple

damped harmonic oscillator model to describe plasmonic resonances, it is possible to explain these shifts as due to plasmon damping.

1. Introduction

Optical antennas are devices designed to efficiently convert optical radiation into localized energy, and vice versa.[1-3] They enhance the interaction between light and matter, and hence hold great promise for applications in physics and chemistry, such as in surface-enhanced Raman spectroscopy[4, 5], single molecular fluorescence[6], nanometric optical trapping[7], biosensing[8, 9], directing of radiation at optical frequency[10-12], optical photolithography[13, 14], and laser applications[15]. Currently, there is great interest in the development of nanostructures that possess additional physical properties that allow combining the optical properties of plasmonic antennas with other structural, electronic, or magnetic properties, thus providing multifunctionality in a single device.[16, 17] Particularly interesting are nanoantennas made of ferromagnetic materials because they combine an optical plasmon resonance with strong magnetic properties.[18] The magnetic behavior can open up the pathway to design new type of biosensors, which can be remotely controlled by external magnetic field.[19] However, plasmons in ferromagnetic materials are typically assumed to exhibit a stronger damping than in noble metals such as gold. A common strategy to overcome this excess damping is to develop hybrid structures consisting of noble metals and ferromagnetic materials, where the noble metal increases the plasmon response[20-23]. These hybrid structures show indeed plasmon-enhanced magneto-optical activity, however, the synthesis requires more tedious fabrication processes. Plasmon properties of pure ferromagnetic nanostructures are a widely

unexplored terrain, although they offer the advantage of stronger magnetic polarication and less demanding fabrication.

In order to estimate theoretically the optical properties of pure nickel nanoparticles, we calculate the polarizibility $\alpha=4\pi a^3(\varepsilon_{Ni}-1)/(\varepsilon_{Ni}+2)$ of a nickel sphere with radius a and dielectric function ε_{Ni}. In quasi-electrostatic approximation ($a<<\lambda$), the field enhancement is proportional to α_{Ni}.[24] Using dielectric data of nickel (**Figure** 1a) from literature [25], we plot α_{Ni} as a function of the wavelength and normalize it to its maximum value. We find a resonance (**Figure** 1b, red solid line) at around 450 nm. Compared to the polarizibility of noble metals such as a gold sphere of equal size (**Figure** 1b, black dashed line α_{Au}), the nickel resonance is weaker owing to the large imaginary part of its dielectric function. However, the plasmon resonance is still a significant optical feature of nickel nanoparticles, which we explore and verify experimentally in this Paper. We identify localized plasmon resonances in circular and elliptical nickel nanoantennas employing near-field microscopy and far-field extinction spectroscopy and discuss the surprisingly large shift between far-and near-field spectra.

2. Results and Discussion

Nickel nanoantennas of different sizes and shapes were fabricated on glass substrates by hole mask colloidal lithography.[26] This method allows for large area bottom-up fabrication of short-range ordered nanostructures. Before characterizing the plasmonic properties of nickel nanostructures, we verified their ferromagnetic functionality by measuring the magneto-optical Kerr effect (MOKE) as a function of an external

magnetic field.[27] The observed hysteresis loops of the disks and ellipsoids clearly reveal the ferromagnetic nature of the nanostructures. (**Figure** 2)

Near-field imaging of the antenna modes was performed with a scattering-type scanning near-field optical microscope (*s*-SNOM) from Neaspec GmbH (www.neaspec.com), operating at λ=633 nm wavelength. (**Figure** 3) Being equipped with a pseudo-heterodyne interferometric detection scheme[28], the microscope allows for mapping both the amplitude E and phase φ of the out-of-plane (normal to the sample surface) electric near-field component at the particle surface. The combined information of amplitude and phase of this component provides a qualitative description of the surface charge density distribution associated with the plasmon oscillations and thus allows for unambiguous mode identification.[29]

In **Figure** 4 we provide experimental evidence of dipolar plasmon modes in nickel circular and elliptical nickel nanoantennas. The far-field extinction spectrum (**Figure** 4a) of the 200 nm spherical disks exhibits a clear resonance peak at around λ = 650 nm. In order to identify the mode associated with the resonance peak, we image amplitude and phase (**Figures**. 4b,c) of the out-of-plane near-field component. In the amplitude image we observe two bright spots aligned along the polarization direction, which are oscillating out of phase for 180°. Such a near-field pattern provides direct experimental evidence of a dipole mode, which has been reported earlier for plasmon-resonant gold disks.[30, 31] A numerical FDTD calculation (Lumerical solutions) of the out-of-plane near-field component (**Figure** 4d) fully confirms the dipolar plasmon mode observed in the near-field images.

For nickel particles with ellipsoidal shape (middle and right-hand side columns of **Figure** 4) we find a strongly anisotropic plasmon response. For a polarization parallel

to the short axis (b = 90 nm), far-field extinction spectroscopy (**Figure** 4a mid-column) reveals a resonance at around λ = 700 nm, which shifts to λ = 1500 nm for a polarization parallel to the long axis (a = 300nm). The near-field amplitude and phase images taken at λ = 633 nm (**Figure** 4b and c mid-column) reveal a clear dipolar mode for a polarization along the short axis (commonly referred to as "transverse" plasmon mode[32]), where the impinging wavelength is close to the plasmon resonance (central column). Comparison with the calculated near-field distribution (**Figure** 4d mid-column) shows an excellent agreement and confirms the dipolar nature of the transverse plasmon mode. The experimental dipolar pattern vanishes when the elliptical antennas are rotated for 90° (right column), as now the imaging wavelength (633nm) is off resonance (**Figure** 4b and c right column). The near fields are stronger for polarization parallel to the short axis of the ellipsoid. This finding provides direct experimental evidence that the near-field strength on the nickel antennas is given by the plasmon excitation rather than by a lightening rod effect. The calculated near-field images (**Figure** 4d right column) reveal the off-resonance dipole mode and confirms that the plasmon fields are much weaker compared to the transverse mode on resonance (**Figure** 4d mid-column). This weak longitudinal dipole mode, however, cannot be identified in the experimental image, which exhibits a homogeneous near-field amplitude and phase contrast. We attribute the homogeneous amplitude and phase signal to the near-field material contrast between nickel and glass substrate. This contrast can be explained simply by a weak near-field interaction between tip and sample, which is not taken into account in the numerical calculations.

In order to gain more detailed insights into the plasmon resonance of nickel antennas, we study nickel disks of different diameters. The far-field extinction spectra (**Figure** 5a) show that the plasmon resonance shifts to longer wavelengths with increasing size, which is similar to the size-dependent resonance shifts in noble metal nanoantennas.[33] For the 100 nm and 200 nm disks, we find the same amplitude and phase patterns as in Figure 4. From the near-field images of amplitude and phase (**Figure** 5c,d) we can thus assign to each resonance peak a dipolar plasmon mode. For the 60nm diameter disks, the imaging wavelength of 633 nm is strongly off resonance. The near fields are weak and distinct dipolar near-field patterns are observed only on a few disks. An interesting observation is made when we compare the near-field images of the 100 nm and 200 nm diameter disks. The near-field amplitude signals are nearly equally strong for both samples (they differ by less than 5%.), even though the imaging wavelength of 633 nm is nearly on resonance for the 200 nm diameter disks but off resonance for the 100 nm diameter disks (see the extinction spectra in **Figure** 5a). This finding indicates significant differences between the far- and near-field spectral response of plasmonic nanostructures[33], which has important implications for the design of efficient nanoantennas.

To explore the spectral differences between the near and far-field properties of the Nickel antennas, we performed further theoretical studies. We numerically calculated the far-field extinction (**Figure** 6a) and near-field spectra (**Figure** 6b) of different nickel disks of 60, 100 and 200 nm diameters on glass. The near-field spectra show the amplitude of the out-of-plane near-field component in a height of 20 nm above the disks. At λ=633 nm wavelengths, the near-field amplitude for the 100 and 200 nm

diameter disks is comparably strong (**Figure** 6b), which is in good agreement with our experimental near-field measurements in **Figure** 5. More importantly, we find that the near-field resonance is dramatically red-shifted compared to the far-field resonance. We note that earlier studies[33, 34] with gold nanoantennas also report spectral shifts Δ_{Au} between the far-and near-field plasmon resonance, however the relative spectral shifts Δ_{Ni} for nickel disks are significantly larger.

The nature of the spectral shifts in plasmonic nanostructures is still a widely unexplored terrain, with only a few studies aiming at unveiling the underlying mechanism. To provide fundamental insights into the origin of this resonance shift, we study the simplest case of a plasmonic particle. We calculate the far-field extinction and near-field amplitude spectra of a small nickel sphere in the quasi-electrostatic approximation (**Figure** 6c), where we can exclude retardation, higher modes or radiation damping. We again find a significant shift between the two spectra, indicating that material intrinsic plasmon damping is the basic mechanism for this effect. To elucidate this phenomenon, we consider the dynamics of the plasmon being a strongly damped, forced harmonic oscillator[35] according to $\ddot{x} + \gamma\dot{x} + \omega_0^2 x = \dfrac{F}{m}\cos\omega t$, where γ is the damping, ω_0 the eigenfrequency, F the driving force and m the mass.[36] The oscillator amplitude $A = \left[\left(\omega_0^2 - \omega^2\right)^2 + \gamma^2\omega^2\right]^{-\frac{1}{2}}$ can be associated with the near-field amplitude E_{loc}/E_{in}, and the energy dissipation of the oscillator $\Delta W = F^2\omega^2\gamma \big/ \left(2m\left[(\omega_0^2 - \omega^2)^2 + \gamma^2\omega^2\right]\right)$ can be associated to the far-field extinction cross section C_{ext}. As shown in **Figure** 6d, the maximum energy dissipation appears at the eigenfrequency ω_0, while the amplitude maximum is shifted to a lower

frequency. The harmonic oscillator model thus clearly explains that the origin of the spectral shift between far- and near-field resonances in small nanoparticles is essentially due to strong plasmon damping. This effect is particularly relevant in nickel antennas because of the imaginary part of the dielectric function. We note that damping may not be the only factor causing the shift. In nanoparticles of finite size, other effects may play a role. It has been reported that with increasing particle size the spectral shift increases, which can be explained by additional damping caused by radiation losses[34]

3. Conclusions

In conclusion, our Paper provides the direct experiment evidence of distinct dipolar plasmon modes in pure ferromagnetic nickel nanoantennas of different sizes and shapes. The simultaneous ferromagnetic and plasmonic dual functionality of nickel opens interesting possibilities for novel applications, such as magnetic manipulation of optical nanoantennas. Moreover, numerical calculations reveal significant differences between far- and near-field spectra of the nickel antennas, which are indicated by comparing single-wavelength near-field images and experimental far-field spectra. We find that the near-field resonance is dramatically red shifted compared to the far-field resonance, an effect that before has not been revealed so clearly in antennas made of standard noble metals. A simple harmonic oscillator model shows that plasmon damping is the major contribution to the shift between near- and far-field resonances. Owning to its strongly damped plasmon, nickel is a well-suited material to explore this phenomenon. Generally, the spectral difference between far- and near-field spectra is an interesting and fundamental property of

plasmonic antennas. This points out the need of taking into account both near-and far-field properties when designing nanophotonic devices.

4. Experimental Section

The scattering-type scanning near-field optical microscope (*s*-SNOM) used in this work is based on a tapping-mode atomic force microscope (AFM) that uses cantilevered tips as near-field probes.[28] (Neaspec GmbH (www.neaspec.com)). For antenna mode imaging we use standard commercial Si tips (Arrow tip, NanoWorld). The tip oscillates at the mechanical resonance frequency $\Omega \approx 300$kHz with an amplitude $\Delta = 30$nm, while the sample is scanned. A laser beam ($\lambda = 632.8$nm) is focused to the tip apex using a parabolic mirror. The backscattered light is analyzed with a pseudo-heterodyne Michelson interferometer, yielding both the amplitude E and phase φ of the backscattered light.[28] Background contributions are suppressed by demodulating the detector signal at a harmonic frequency $n\Omega$ ($n\geq2$), yielding background free near-field amplitude and phase images. In order to avoid distortion of the plasmon modes by near-field coupling between antenna and tip, we illuminate the sample with s-polarized light. In this scheme, the incident light efficiently polarizes the nickel antennas but not the AFM tip.[31, 37] In the presented experiments, the p-polarized backscattered light is selected by a vertically aligned polarizer in front of the detector (Polarizer 1). To achieve interference between the s-polarized incident light and the detected p-polarized backscattered light, a 45 degree rotated polarizer (Polarizer 2) is placed in between the vibrating reference mirror and the beam splitter.

[1]   K. B. Crozier, A. Sundaramurthy, G. S. Kino,C. F. Quate, *J. Appl. Phys.* **2003**, *94*,4632.

[2]   R. D. Grober, R. J. Schoelkopf,D. E. Prober, *Appl. Phys. Lett.* **1997**, *70*,1354.

[3]   P. Muhlschlegel, H. J. Eisler, O. J. F. Martin, B. Hecht,D. W. Pohl, *Science* **2005**, *308*,1607.

[4]   K. Kneipp, Y. Wang, H. Kneipp, L. T. Perelman, I. Itzkan, R. Dasari,M. S. Feld, *Phys. Rev. Lett.* **1997**, *78*,1667.

[5]   H. X. Xu, E. J. Bjerneld, M. Kall,L. Borjesson, *Phys. Rev. Lett.* **1999**, *83*,4357.

[6]   A. Kinkhabwala, Z. F. Yu, S. H. Fan, Y. Avlasevich, K. Mullen,W. E. Moerner, *Nat. Photonics* **2009**, *3*,654.

[7]   L. Novotny, R. X. Bian,X. S. Xie, *Phys. Rev. Lett.* **1997**, *79*,645.

[8]   A. J. Haes, W. P. Hall, L. Chang, W. L. Klein,R. P. Van Duyne, *Nano Lett.* **2004**, *4*,1029.

[9]   J. N. Anker, W. P. Hall, O. Lyandres, N. C. Shah, J. Zhao,R. P. Van Duyne, *Nat. Mater.* **2008**, *7*,442.

[10]   J. N. Farahani, D. W. Pohl, H. J. Eisler,B. Hecht, *Phys. Rev. Lett.* **2005**, *95*,017402.

[11]   T. H. Taminiau, F. D. Stefani, F. B. Segerink,N. F. Van Hulst, *Nat. Photonics* **2008**, *2*,234.

[12]   A. G. Curto, G. Volpe, T. H. Taminiau, M. P. Kreuzer, R. Quidant,N. F. van Hulst, *Science* **2010**, *329*,930.

[13]   A. Sundaramurthy, P. J. Schuck, N. R. Conley, D. P. Fromm, G. S. Kino,W. E. Moerner, *Nano Lett.* **2006**, *6*,355.

[14]   W. Srituravanich, N. Fang, C. Sun, Q. Luo,X. Zhang, *Nano Lett.* **2004**, *4*,1085.

[15]   E. Cubukcu, E. A. Kort, K. B. Crozier,F. Capasso, *Appl. Phys. Lett.* **2006**, *89*,093120.

[16]   N. Insin, J. B. Tracy, H. Lee, J. P. Zimmer, R. M. Westervelt,M. G. Bawendi, *ACS Nano* **2008**, *2*,197.

[17]   K. C. Weng, C. O. Noble, B. Papahadjopoulos-Sternberg, F. F. Chen, D. C. Drummond, D. B. Kirpotin, D. H. Wang, Y. K. Hom, B. Hann,J. W. Park, *Nano Lett.* **2008**, *8*,2851.

[18]   C. S. Levin, C. Hofmann, T. A. Ali, A. T. Kelly, E. Morosan, P. Nordlander, K. H. Whitmire,N. J. Halas, *ACS Nano* **2009**, *3*,1379.

[19]   A. V. S. Ventsislav K. Valev, Werner Gillijns, Yogesh Jeyaram, Hanna Paddubrouskaya, Alexander Volodin, Claudiu G. Biris, Nicolae C. Panoiu, Ben De Clercq, Marcel Ameloot, Oleg A. Aktsipetrov, Victor V. Moshchalkov, Thierry Verbiest, *ACS Nano* **2011**, *5*,91.

[20]   N. J. Halas, *MRS Bull.* **2005**, *30*,362.

[21]   H. Wang, D. W. Brandl, P. Nordlander,N. J. Halas, *Accounts Chem. Res.* **2007**, *40*,53.

[22]   V. V. Temnov, G. Armelles, U. Woggon, D. Guzatov, A. Cebollada, A. Garcia-Martin, J. M. Garcia-Martin, T. Thomay, A. Leitenstorfer,R. Bratschitsch, *Nat. Photonics*, **2010**,*4*,107.

[23]   J. B. Gonzalez-Diaz, A. Garcia-Martin, G. Armelles, D. Navas, M. Vazquez, K. Nielsch, R. B. Wehrspohn,U. Gosele, *Adv. Mater.* **2007**, *19*,2643.

[24]   J. D. Jackson, *Classical Electrodynamics*, Wiley & Sons, New York **1975**

[25] E. W. Palik, *Handbook of Optical Constants of Solids*, Academic, San Diego **1985**

[26] H. Fredriksson, Y. Alaverdyan, A. Dmitriev, C. Langhammer, D. S. Sutherland, M. Zaech,B. Kasemo, *Adv. Mater.* **2007**, *19*,4297.

[27] P. Vavassori, *Appl. Phys. Lett.* **2000**, *77*,1605.

[28] N. Ocelic, A. Huber,R. Hillenbrand, *Appl. Phys. Lett.* **2006**, *89*,101124.

[29] M. Schnell, A. Garcia-Etxarri, J. Alkorta, J. Aizpurua,R. Hillenbrand, *Nano Lett.* **2010**, *10*,3524.

[30] R. Hillenbrand, F. Keilmann, P. Hanarp, D. S. Sutherland,J. Aizpurua, *Appl. Phys. Lett.* **2003**, *83*,368.

[31] R. Esteban, R. Vogelgesang, J. Dorfmuller, A. Dmitriev, C. Rockstuhl, C. Etrich,K. Kern, *Nano Lett.* **2008**, *8*,3155.

[32] S. Link,M. A. El-Sayed, *J. Phys. Chem. B* **1999**, *103*,8410.

[33] G. W. Bryant, F. J. G. De Abajo,J. Aizpurua, *Nano Lett.* **2008**, *8*,631.

[34] B. M. Ross,L. P. Lee, *Opt. Lett.* **2009**, *34*,896.

[35] J. Zuloaga,P. Nordlander, *Nano Lett.* **2011**, *11*,1280.

[36] D. R. H. Craig F. Bohren, *Absorption and Scattering of Light by Small Particles*, John Wiley & Sons, iNC. **1998**

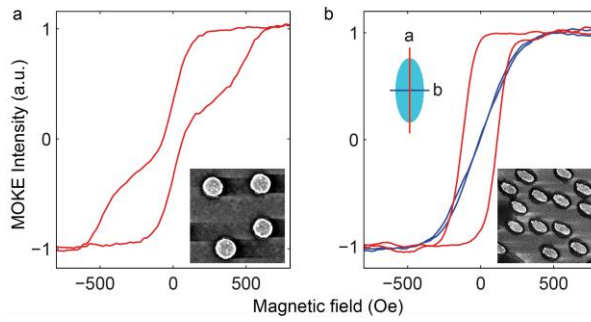[37] D. S. Kim, J. Heo, S. H. Ahn, S. W. Han, W. S. Yun,Z. H. Kim, *Nano Lett.* **2009**, *9*,3619.
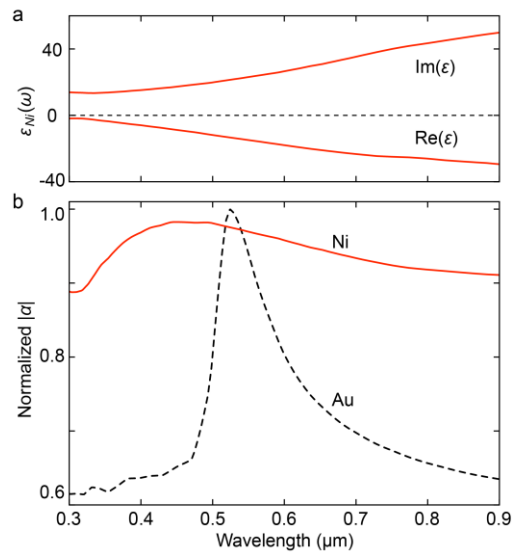
Figure 1. (a) Dielectric function of nickel taken from Palik. (b) Comparison of the polarizibility $|\alpha|$ of nickel and gold sphere.

Figure 2. (a) MOKE hysteresis loops of nickel disks (diameter = 200nm) (b) MOKE hysteresis loops of nickel ellipsoids (long axis length a = 300nm, short axis length b = 90nm). The red and blue curves correspond to the easy and hard magnetization axes of elliptical nickel antennas. Scanning electronic microscopy (SEM) images are shown as insets.
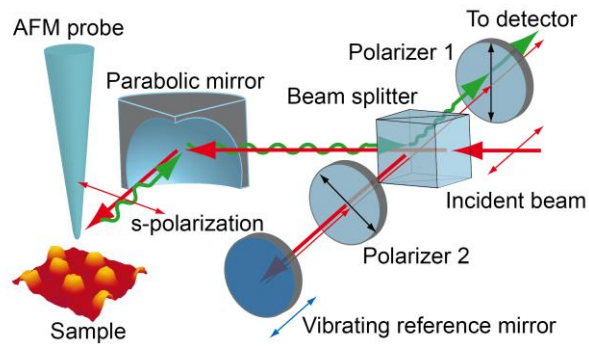
Figure 3. Scattering-type scanning near-field optical microscope (*s*-SNOM). The basis is a tapping-mode atomic force microscope (AFM) that uses cantilevered tips as near-field probes. The incoming light is s-polarized. The p-polarized backscattered light is recorded with a pseudo-heterodyne Michelson interferometer,[27] yielding both the amplitude E and phase φ of the vertical (out-of-plane) near-field component.
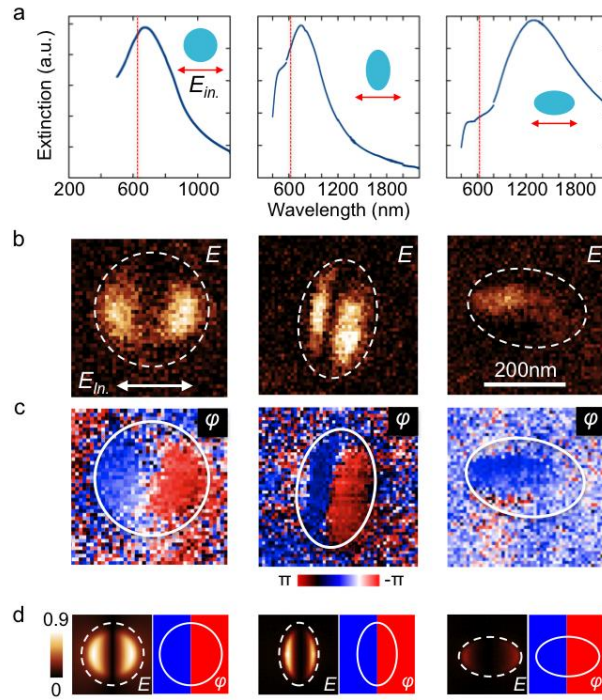
Figure 4. (a) Normalized extinction spectra. Left: of 200 nm diameter nickel disks. Center: of nickel ellipsoids with polarization along the short axis (b = 90 nm). Right: of nickel ellipsoids with polarization along the long axis (a = 300 nm). The red lines in the spectra mark the near-field imaging wavelength. (b) Near-field amplitude images. The arrow and bar denote the polarization of incident laser beam, respectively the scale of the images. (c) Near-field phase images. (d) FDTD calculated near-field amplitude $E = E_{loc}/E_{in}$ and phase φ maps at 633nm. The white circles in the near-field amplitude and phase images outline the nickel antennas.
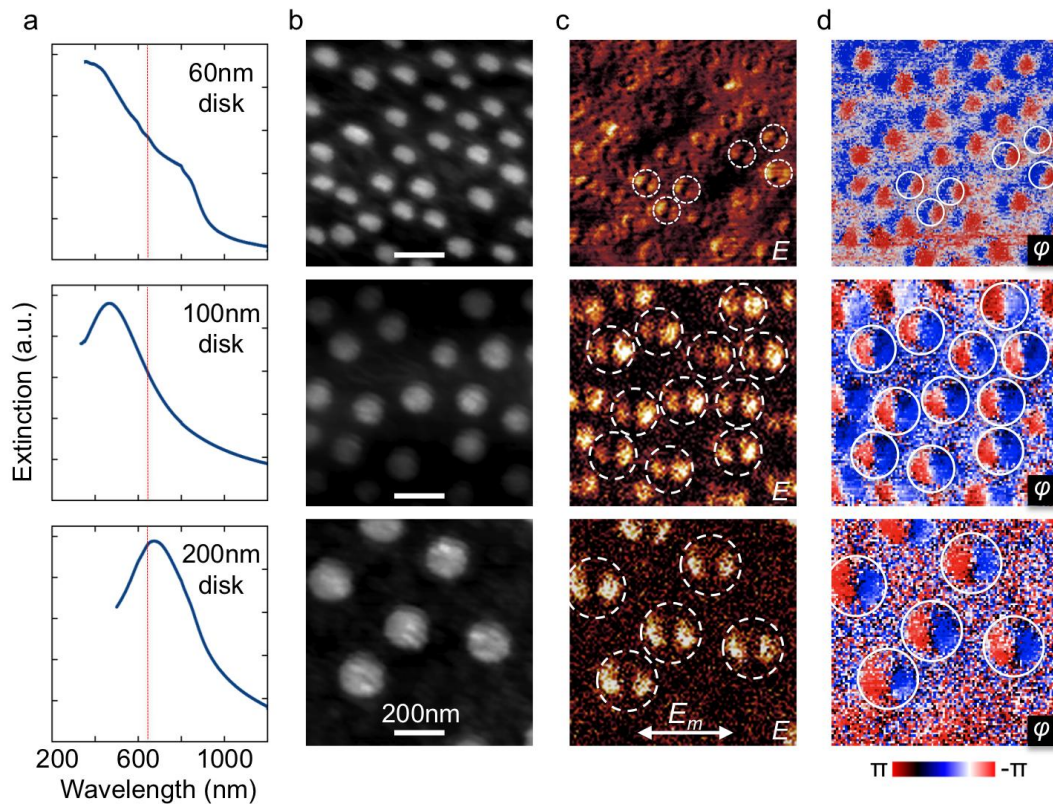
Figure 5. (a) Normalized extinction spectra of nickel disks of diameter d = 60, 100, 200nm, respectively. The red line in the spectra marks the near-field imaging wavelength. (b) Topography images. The elliptical shape of 60nm disk is due to sample drift during imaging. (c) Near-field amplitude images. (d) Near-field phase images. The white circles in the near-field amplitude and phase images outline the positions of nickel disks.
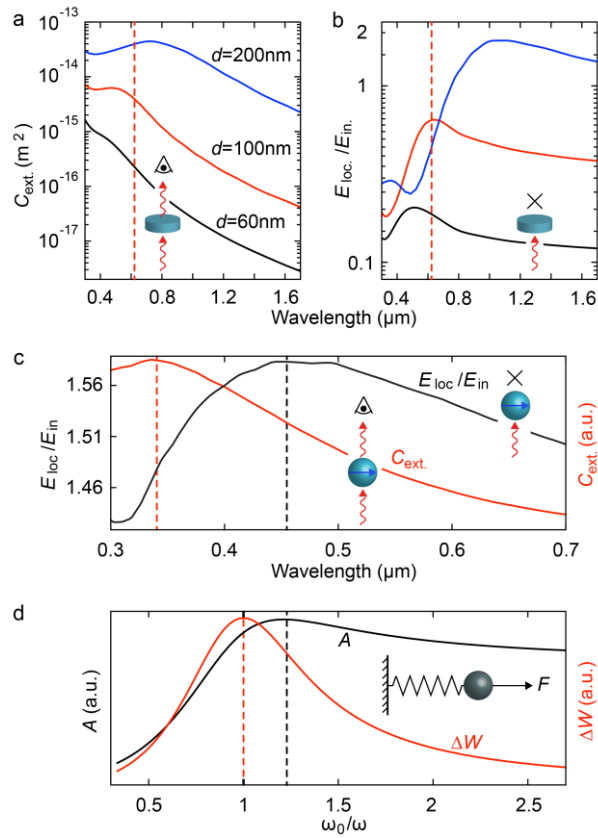
Figure 6. (a) Theoretical extinction spectra C_{ext} and (b) near-field spectra E_{loc}/E_{in} (out-of-plane component) of nickel disks of diameter d = 60, 100, 200nm respectively. The red dashed lines in (a) and (b) mark the near-field imaging wavelength. (c) Calculated extinction and near-field spectra of a small nickel sphere of diameter d = 10nm. (d) Calculated amplitude A and dissipation spectra ΔW according to harmonic oscillator model.

The table of contents entry

Experimental evidence of plasmon resonances in pure nickel nanoantennas is provided by both far-field spectroscopy and near-field microscopy. Ultra-high resolution near-field microscopy visualizes for the first time the transverse plasmon mode of elongated nanoantennas. We furthermore describe the shifts between far- and near-field spectra of plasmonic antennas, which points out the need of taking into account both near- and far-field properties when designing nanophotonic devices.

TOC Keyword: plasmonics, optical antennas, magnetic nanoparticles, near-field optical imaging, scattering-type scanning near-field optical microscopy

J. Chen, P. Albella, Z. Pirzadeh, P. Alonso-González, F. Huth, S. Bonetti, V. Bonanni, J. Åkerman, J.Nogués, P. Vavassori, A. Dmitriev, J. Aizpurua, R. Hillenbrand*

Title: Plasmonic Nickel Nanoantennas

ToC figure
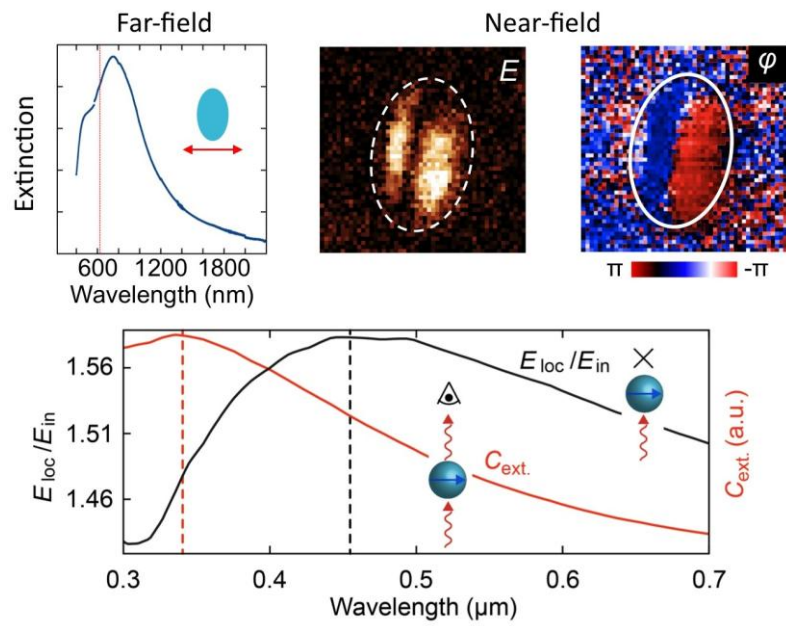
Page Headings

Left page: Jianing Chen et al.

Right page: Plasmonic Nickel Nanoantennas